

Growth and characterization of magnetite-maghemite thin films by the dip coating method

A. A. Velásquez¹  · A. Arnedo¹

© Springer International Publishing Switzerland 2017

Abstract We present the process of growth and characterization of magnetite-maghemite thin films obtained by the dip coating method. The thin films were deposited on glass substrates, using a ferrofluid of nanostructured magnetite-maghemite particles as precursor solution. During the growth of the films the following parameters were controlled: number of dips of the substrates, dip velocity of the substrates and drying times. The films were characterized by Atomic Force Microscopy, Scanning Electron Microscopy, four-point method for resistance measurement, Room Temperature Mössbauer Spectroscopy and Hall effect. Mössbauer measurements showed the presence of a sextet attributed to maghemite (γ - Fe_2O_3) and two doublets attributed to superparamagnetic magnetite (Fe_3O_4), indicating a distribution of oxidation states of the iron as well as a particle size distribution of the magnetic phases in the films. Atomic force microscopy measurements showed that the films cover quasi uniformly the substrates, existing in them some pores with sub-micron size. Scanning Electron Microscopy measurements showed a uniform structure in the films, with spherical particles with size around 10 nm. Voltage versus current measurements showed an ohmic response of the films for currents between 0 and 100 nA. On the other hand, Hall effect measurements showed a nonlinear response of the Hall voltage with the magnetic flux density applied perpendicular to the plane of the films, however the response is fairly linear for magnetic flux densities between 0.15 and 0.35 T approximately. The results suggest that the films are promising for application as magnetic flux density sensors.

Keywords Thin films · Magnetite · Dip coating · Ferrofluids · Mössbauer spectroscopy

This article is part of the Topical Collection on *Proceedings of the 15th Latin American Conference on the Applications of the Mössbauer Effect (LACAME 2016), 13-18 November 2016, Panama City, Panama*
Edited by Juan A. Jaén

✉ A. A. Velásquez
avelas26@eafit.edu.edu.co

¹ Grupo de Electromagnetismo Aplicado, Universidad EAFIT, A.A. 3300, Medellín, Colombia

1 Introduction

Magnetite thin films are systems very promising for technological applications such as optical polarizers and birefringence induced systems [1, 2], Hall effect sensors [3, 4], magnetoresistive sensors [5], among others. On the other hand, these systems are having increasing interest because their applications as half-metals spin polarized media, suitable for magnetic recording devices and logic computation systems [6]. There are several methods for obtaining these films, such as magnetron sputtering [7, 8], reactive evaporation [9], sol-gel [10, 11], among others, however the humid methods, such as dip coating offer important advantages, among them are the simplicity and low cost of the implementation of the system for the growth of the films. In the dip coating technique the thickness of the films can be controlled by selecting the proper number of dips of the substrate in the precursor solution and the adherence of the films to the substrate can be improved by promoting a well bonding between the substrate ions and the surface ions of the nanoparticles which compose the precursor solution.

In this work we present a low cost method to obtain magnetic thin films by the dip coating technique, using a ferrofluid composed by nano-magnetite and nano-maghemite particles as precursor solution. The magnetic, structural and electrical characteristics of the films obtained are discussed in the following sessions.

2 Experimental

2.1 Preparation of the ferrofluid

As precursor solution of the thin films we used a ferrofluid composed by nanoparticles of magnetite (Fe_3O_4) and its high oxidized state of maghemite ($\gamma\text{-Fe}_2\text{O}_3$). For the synthesis of the ferrofluid we employed the coprecipitation method described by Lin, Lee and Chiu [12] as follows: 100.0 mL of solution 6×10^{-2} M in Fe^{2+} and 12×10^{-2} M in Fe^{3+} were added dropwise in 100.0 mL of 0.4 % sodium polyacrylate solution, with constant stirring at 600 rpm and deaerating with $\text{N}_2(\text{g})$ to prevent oxidation of the Fe^{2+} ions before the formation of crystals. The concentration of Fe^{3+} and Fe^{2+} was adjusted to 2:1 locking for obtaining a well stoichiometric magnetite. The pH of the reaction was kept at 12 by controlled addition of 1×10^{-1} M NaOH solution by using a titration equipment model Titrando 902 from Metrohm. After completing the addition of the iron solution, the dark brown precipitate of magnetic nanoparticles was kept under magnetic stirring during 1 hour. Later, the magnetic fluid was washed with deionized water using a dialysis membrane until the conductivity of wash water was the same as the conductivity of the water deionized. Afterward the ferrofluid obtained was stored in an assay tube for the subsequent dip coating experiments. The Fig. 1 shows a view of the response of the ferrofluid to a magnetic field generated by a permanent magnet.

2.2 Preparation of the substrates

As substrate of the film, we cut glass microscope slides of 1 cm side. In order to promote a good adherence of the films to the substrates, these were immersed in an aqueous 5M alkaline solution of KOH under sonication during 30 minutes. An ultrasound bath model Branson 1800 with sonication frequency of 40 kHz was employed for this purpose. After this process the substrates were washed with deionized water and dried in an oven at 60 °C

Fig. 1 Response of the ferrofluid to a permanent magnetic field



for 2 hours. The etching of the substrates with the KOH solution was implemented locking for a well bonding between the surface charge of the magnetic nanoparticles and SiOH_2^+ groups present in the surface of the glass substrate for the concentration of KOH employed.

2.3 Growth of the films

For the growth of the films we used a dip coating equipment developed in our laboratory [13], which is presented in Fig. 2. This equipment allows control of the following parameters of the process: number of dips (n), dip velocity (v_{dip}), dip time (t_{dip}) and drying time (t_{drying}) of the films. After several assays, the most uniform films were obtained with the following set of parameters: $n = 7$ dips, $v_{dip} = 3$ mm/s, $t_{dip} = 10$ s and $t_{drying} = 300$ s. Two films grown under this set of parameters were selected for the experiments presented in the subsequent sections. For sake of brevity, in those cases where no significant differences were observed in the characterization of the two films, only the results obtained with one of the films are presented.

2.4 Experimental techniques

Surface topography micrographs of the films were taken with an atomic force microscope model easyScan 2 from Nanosurf. The morphology and particle size were analyzed with a field emission scanning electron microscope JEOL JSM-6701F, with acceleration voltage of 8 kV and magnifications between 140,000 and 450,000. The magnetic phases and hyperfine interactions in the particles of the films were studied by room temperature transmission Mössbauer spectroscopy by using a Mössbauer spectrometer developed in our laboratory [14]. This spectrometer operates in the mode of constant acceleration, with a radioactive source of $^{57}\text{Co}(\text{Rh})$ with initial activity of 25 mCi and velocities between -12 mm/s and 12 mm/s. The absorber, composed by the film and the glass substrate, was placed between the source and the radiation detector LND 45431 for these measurements. The electrical properties of the films were characterized by the van der Pauw method [15]. For these measurements we placed thin copper wire terminals in the corners of the films with silver

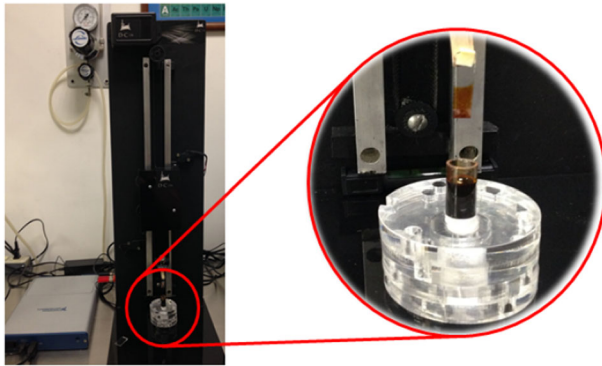


Fig. 2 View of the dip coating experiment employed to grow the thin films

paint. Afterward we applied current between two terminals and measured the voltage in the other two terminals. We programmed current ramps with steps of 5 nA by using a KEITHLEY 6221 source, limiting the maximum current applied to the films to 100 nA in order to prevent overheating of the films by Joule effect. The voltage measurements were realized with a nanovoltmeter KEITHLEY 2182A. The two devices were interconnected with each other and then connected to a computer through a communication interface IEEE 488-USB from National Instruments. We automated and controlled all measurements from a computer through a user graphical interface developed in LabVIEW software. For the Hall measurements small copper contacts were placed in the center of the edges of the films, a constant current was applied between two contacts placed in opposite edges of the film while the Hall voltage was measured between opposite contacts aligned in perpendicular direction. The plane of the film was placed perpendicular to the magnetic flux density generated in the gap region of an electromagnet GMW Associates 3470. The experiment was automated by programming successive increments of the magnetic flux density and measuring the Hall voltage with the nanovoltmeter KEITHLEY 2182A.

3 Results and discussion

3.1 Surface morphology of the films

An AFM micrograph of the films, obtained in topographical mode, is presented in Fig. 3. This image shows that the film covers quasi uniformly the substrate. The dark zones observed in the image correspond to pores, whose mean diameter was estimated at $0.25 \mu\text{m}$. The three-dimensional view of the film presented in Fig. 3b shows some acute mounds, which are attributed to aggregates of nanoparticles in the precursor ferrofluid. The root mean square rugosity of the film estimated from AFM measurements was 15 nm.

To estimate the thickness of the films, a portion of these was detached from the substrates with a sharp object. Afterward a topographical micrograph was taken near to the interface film-substrate, as presented in Fig. 4. The points of the image along the segment indicated in Fig. 4a were processed with the software SPIP from nanoScience®, which allowed us to obtain the profile of the step film-substrate presented in Fig. 4b. From this profile, we estimated the thickness of the film at 480 nm.

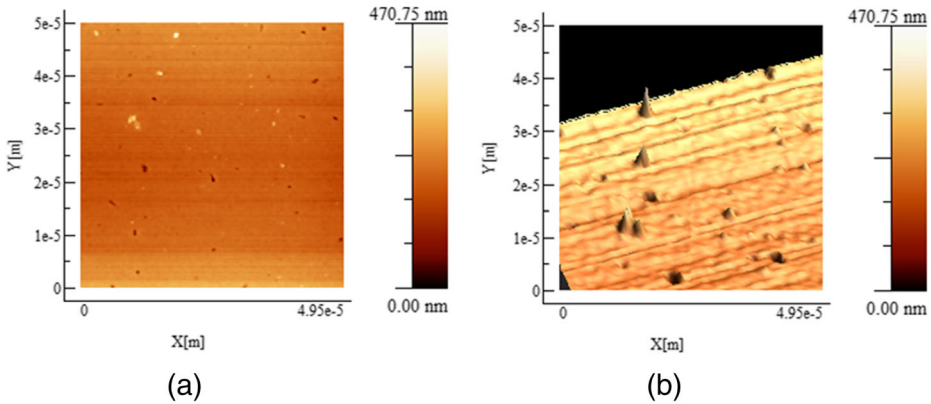


Fig. 3 Topographical AFM micrograph of the film. **a** Two-dimensional view, **b** Three-dimensional view

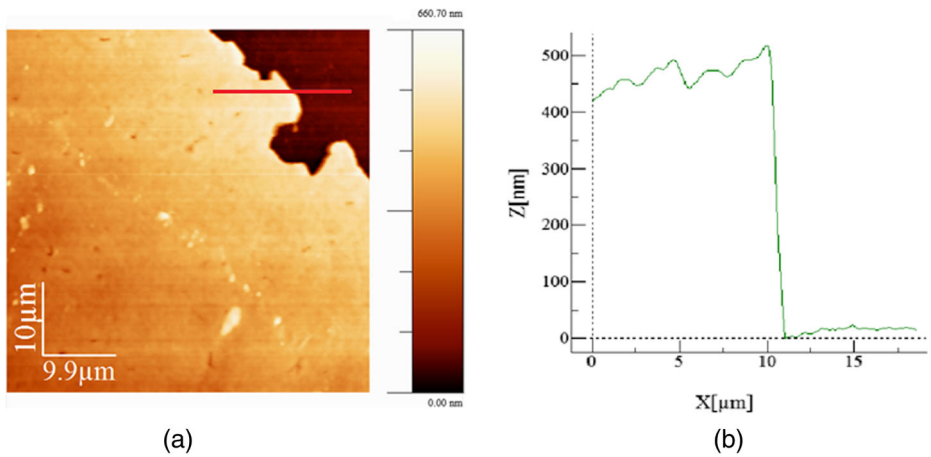


Fig. 4 Estimation of the thickness of the films from AFM micrographs. **a** Micrograph taken around the film/substrate region, **b** Profile of the image in direction perpendicular to the film along the film/substrate segment indicated in (a)

3.2 Scanning electron microscopy measurements

The Fig. 5 presents two micrographs of the film at different magnifications, these images evidence a dense cover of the substrate, as well as some cracks whose width was around 70 nm. The morphology of the particles was almost spherical, with particle sizes ranging from 9 nm and 16 nm approximately.

3.3 Voltage versus current measurements

The scheme of the four-point experiment used to measure the electrical response of the films is presented in Fig. 6. The measurements were made by applying current between two corners of the films and measuring the voltage drop between the opposite two corners. The voltage drop was measured again by inverting the current, and subsequently calculating the

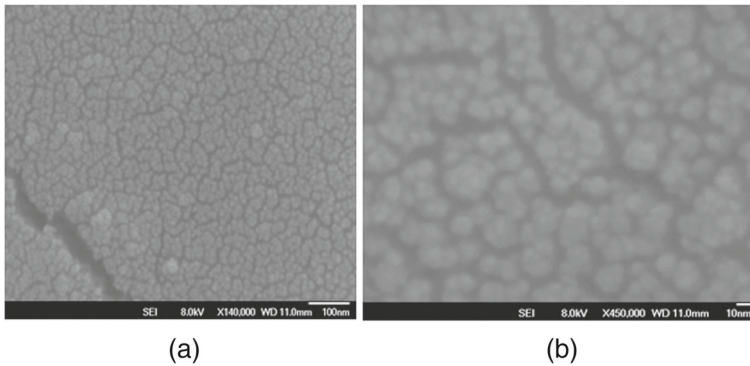


Fig. 5 SEM micrographs of the film. **a** View of the film with a magnification of 140k, **(b)** Detail of the morphology and particle size with a magnification of 450k

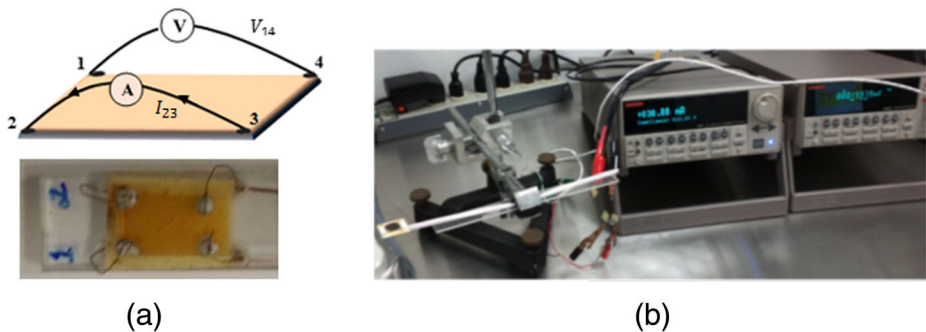


Fig. 6 Four point experiment to measure the electrical response of the films. **a** Scheme of the experiment and connections in one of the films, **(b)** Experimental setup used to make the measurements

semi difference between the voltages in order to cancel the thermal voltage induced in the contact points of the film with the measurement copper probes.

The Fig. 7 shows the curves Voltage vs Current for two similar films obtained after 7 dips. Both curves show a fairly linear relationship between voltage and current, indicating an ohmic response of the films to the electrical stimuli. In both cases the sheet electrical resistance of the films was around $R_s = 190 \Omega$. We attribute the conductivity of the films to the hopping current caused by thermally activated electrons which occupy orbitals of Fe^{2+} and Fe^{3+} ions placed in neighboring octahedra in the lattice structure of magnetite, generating a non-equilibrium of the oxidation states of these ions, which favors the current flow through the material.

3.4 Mössbauer spectroscopy measurements

Room temperature Mössbauer spectra of two films are presented in Fig. 8. The spectra were very similar and both were well fitted with one sextet and two doublets with Lorentzian line profile, whose spectral parameters are presented in Table 1. We employed the least square software MOSFIT [16] for fitting the spectra, freeing all spectral parameters during the fitting process. The hyperfine parameters of both spectra did not present significant variations

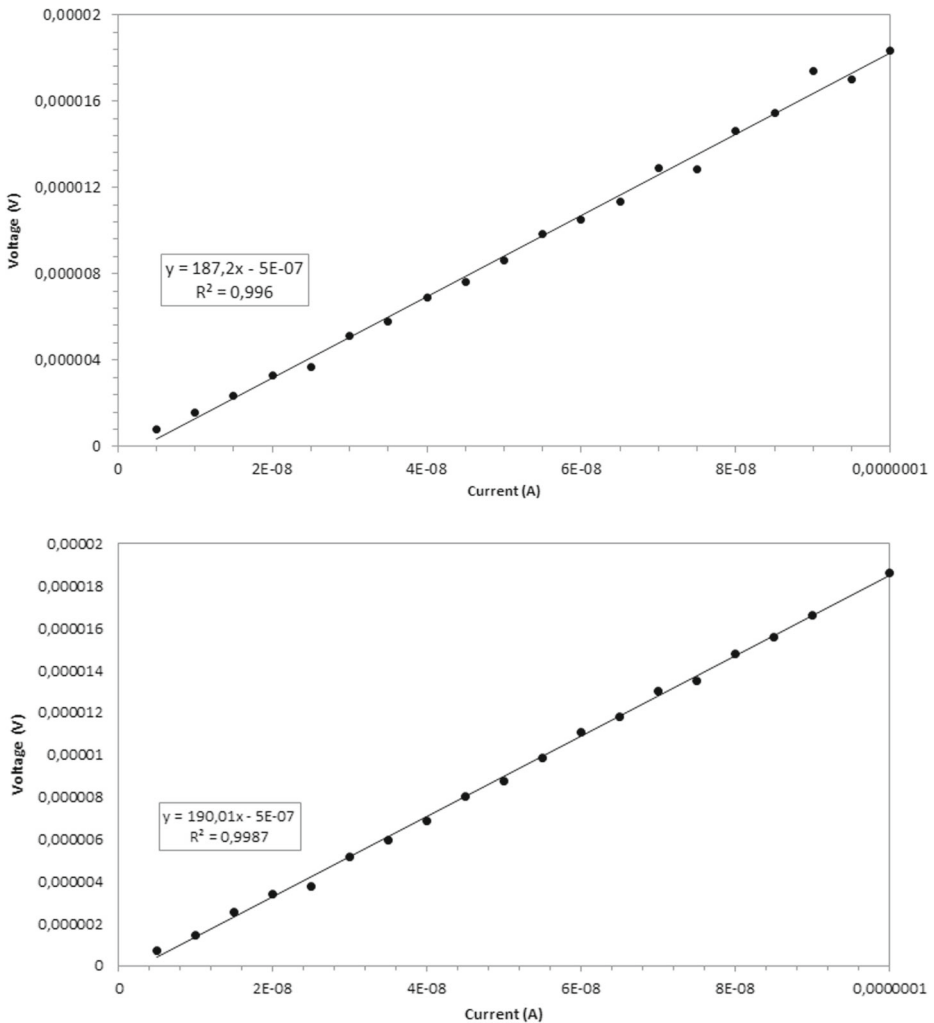


Fig. 7 Voltage versus current curves of two similar films, obtained by the four-point method

and they agree between the errors bars reported. Mössbauer measurements show that the films are composed by a mixture of magnetite and its high oxidized state of maghemite, both phases having different particle size, evidenced by the coexistence of sextets and doublets in the spectra. The sextet is attributed to Fe^{3+} ions in maghemite ($\gamma-Fe_2O_3$), the first doublet is attributed to Fe^{3+} ions in superparamagnetic magnetite-maghemite and the second doublet is attributed to $Fe^{2.5+}$ ions at octahedral sites of this superparamagnetic magnetite (Fe_3O_4), where hopping current between Fe^{3+} and Fe^{2+} ions occupying neighboring octahedral sites takes place. Magnetite and maghemite can coexist in the films because the oxidation of Fe^{2+} is favored during the drying stages of the dip coating process, where the aqueous solvent of the ferrofluid evaporates from the films. Ions Fe^{3+} of magnetite and maghemite have similar hyperfine parameters, so their sub spectra overlap in the Mössbauer spectra.

An isomer shift around 0.26 mm/s is expected for Fe^{3+} ions in magnetite and maghemite, however it is important to note that in the ferrofluid the nanoparticles are surrounded by

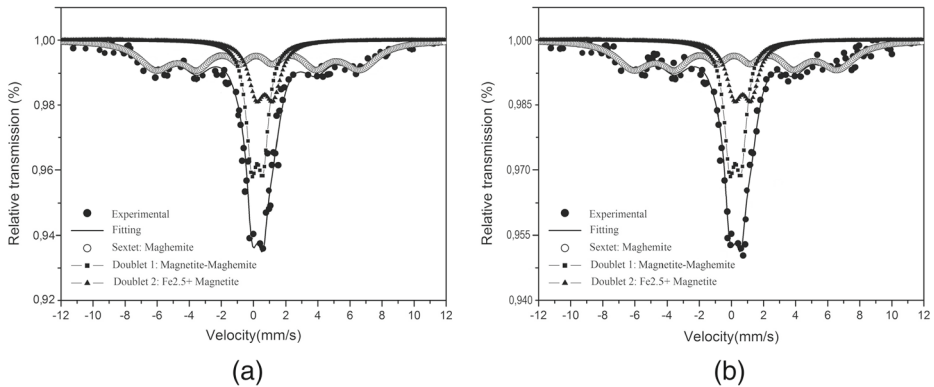


Fig. 8 Typical room temperature Mössbauer spectra of the films

Table 1 Mössbauer parameters of the iron phases identified in the films

Film	Subspectrum	Phase	B_{hf} (T)	IS(mm/s)	QS(mm/s)	W(mm/s)	A(%)
(a)	Sextet	$\gamma\text{-Fe}_2\text{O}_3$	38.5 ± 0.2	0.36 ± 0.02	0.02 ± 0.02	0.85 ± 0.02	39
	Doublet 1	Fe^{3+} ($\text{Fe}_3\text{O}_4\text{-}\gamma\text{-Fe}_2\text{O}_3$)		0.36 ± 0.02	0.57 ± 0.02	0.71 ± 0.02	36
	Doublet 2	$\text{Fe}^{2.5+}$ (Fe_3O_4)		0.61 ± 0.02	0.64 ± 0.02	0.73 ± 0.02	25
(b)	Sextet	$\gamma\text{-Fe}_2\text{O}_3$	38.4 ± 0.2	0.35 ± 0.02	0.02 ± 0.02	0.87 ± 0.02	41
	Doublet 1	Fe^{3+} ($\text{Fe}_3\text{O}_4\text{-}\gamma\text{-Fe}_2\text{O}_3$)		0.36 ± 0.02	0.56 ± 0.02	0.70 ± 0.02	35
	Doublet 2	$\text{Fe}^{2.5+}$ (Fe_3O_4)		0.63 ± 0.02	0.66 ± 0.02	0.70 ± 0.02	24

Convention for the parameters is: B_{hf} hyperfine magnetic field, IS isomer shift relative to $\alpha\text{-Fe}$, QS quadrupole splitting, A: spectral area

polyacrylate chains, which modify their surface charge in order to provide the repulsive ionic force to compensate the magnetic force which tends to aggregate them. The surface charge accumulated on the surface of the nanoparticles can screen the effective charge which interacts with the nuclear charge in ^{57}Fe resonant atoms, increasing their isomer shift with respect to the usual values for Fe^{3+} in spinel structures, which can explain the higher value of 0.36 mm/s observed in the spectrum.

For a crystalline and stoichiometric magnetite, the ratio $R=A(\text{Fe}^{2.5+})/A(\text{Fe}^{3+})$ of the areas of the sub spectra associated to $\text{Fe}^{2.5+}$ and Fe^{3+} is around 1.8 [17], however this ratio is not expected for the ferrofluids employed in this work, because the partial oxidation of Fe^{2+} ions at octahedral sites increases the population of Fe^{3+} in the particles, which in turns increases the spectral area $A(\text{Fe}^{3+})$, decreasing in this way the ratio R.

3.5 Hall effect measurements

The details of the experiment developed to measure the Hall voltage induced in the films is presented in Fig. 9. The films were placed in the middle point of the air gap between the poles of the electromagnet in order to ensure a homogeneous magnetic flux density in all surface of the film.

For making the Hall effect measurements, we applied a constant current of 50 nA between the terminals 1 and 3 schematized in Fig. 9a, subsequently we measured the voltage drop between the terminals 4 and 2. The results of the Hall measurements for $0 \leq B \leq 0.5$ T,

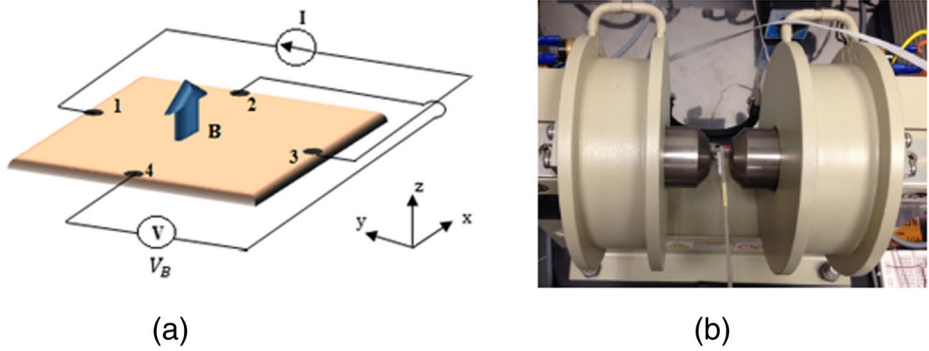


Fig. 9 Experiment to perform the Hall effect measurements in the thin films. **a** Scheme of the experiment, **(b)** Experimental setup used to make the measurements

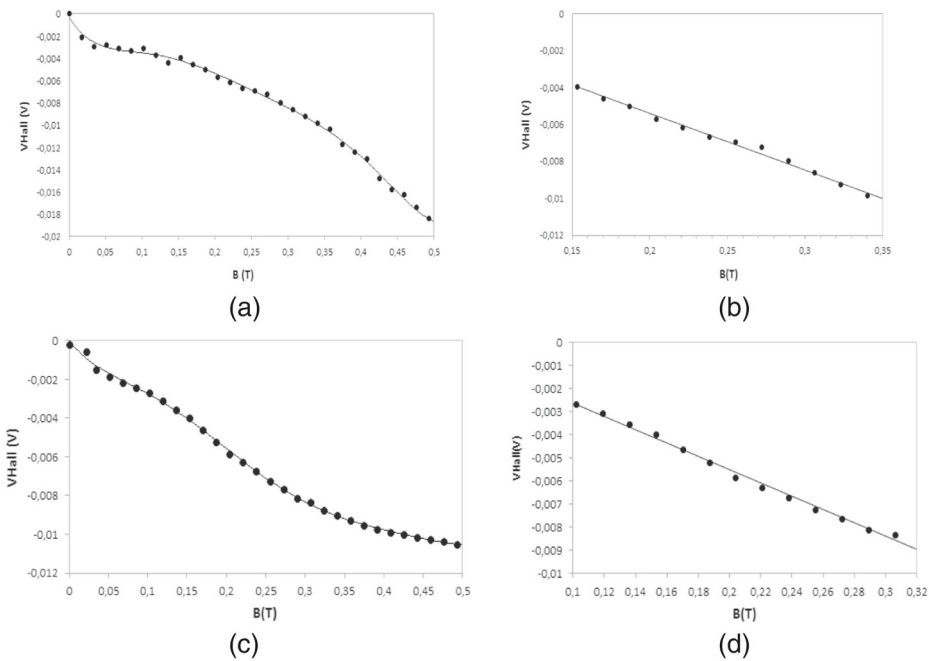


Fig. 10 **a,c** Results of the Hall measurements in the films, **(b,d)** linearization of the respective Hall signals in the intervals $0.15 \text{ T} \leq B \leq 0.35 \text{ T}$ and $0.11 \text{ T} \leq B \leq 0.31 \text{ T}$

being 0.5 T the maximal flux density obtained with the pole separation employed, are presented in Fig. 10.

The curves of the Hall voltage vs. magnetic flux density of the two films were well fitted with the following sixth-order polynomials:

$$V_H = 38,125B^6 - 59,505B^5 + 35,818B^4 - 10,486B^3 + 1,4817B^2 - 0,1057B - 0,0003 \tag{1}$$

$$V_H = 13,313B^6 - 22,576B^5 + 14,406B^4 - 4,1764B^3 + 0,5378B^2 - 0,0518B + 0,00002 \quad (2)$$

With a determination coefficients $R^2 = 0,9977$ and $R^2 = 0,9985$, respectively.

In the first film a linear dependence is evidenced in the interval $0.15 \text{ T} \leq B \leq 0.35 \text{ T}$, which is well described by the equation:

$$V_H = -0,0307B + 0,0007 \quad (3)$$

With a determination coefficient $R^2 = 0,9934$.

In the second film a linear dependence is evidenced in the interval $0.1 \text{ T} \leq B \leq 0.31 \text{ T}$, which is well described by the equation:

$$V_H = -0,0286B + 0,0002 \quad (4)$$

With a determination coefficient $R^2 = 0,9942$.

The Hall sensitivity, given by the slope of the linear curves has a relative variation of 6.8 % between the two films. This variation can be attributed to microstructural difference in the films, due to pores, cracks, local difference in the thickness and aggregation of the magnetic particles of the ferrofluid during the dry process, among other effects observed.

The sign of the Hall voltage is consistent with the conduction of negative carriers in the films, in our case the electrons, which perform hopping between neighboring octahedra as well as inter-grain tunneling. These electrons are also responsible for the ohmic conductivity of the films observed in the voltage versus current measurements. According to the literature [3, 4], the relation for the Hall voltage in a ferromagnetic and conductive thin film is given by:

$$V_H = \frac{\mu_o (R_0 H_{\perp} + R_A M_{\perp}) I}{t} = \frac{\rho_H}{t} I \quad (5)$$

Where:

V_H : Hall voltage induced in the terminals of the film.

μ_o : magnetic permeability of the free space.

R_0 : ordinary Hall coefficient of the material of the film.

R_A : anomalous Hall coefficient of the material of the film.

t : thickness of the film.

H_{\perp} : magnetic field applied perpendicular to the direction of the current.

M_{\perp} : magnetization of the film perpendicular to the direction of the current.

I : intensity of current applied to the film.

$\rho_H = \mu_o (R_0 H_{\perp} + R_A M_{\perp})$: Hall resistivity.

In the linear region of the curve, obtained for $0.15 \text{ T} \leq B \leq 0.35 \text{ T}$, we can suppose that M_{\perp} is proportional to the applied magnetic field, being the constant of proportionality equal to the magnetic susceptibility χ_{\perp} perpendicular to the plane of the film. In this case the (1) can be written as:

$$\begin{aligned} V_H &\approx \frac{\mu_o (R_0 H_{\perp} + R_1 \chi_{\perp} H_{\perp}) I}{t} = \frac{\mu_o H_{\perp} (R_0 + R_1 \chi_{\perp}) I}{t} \\ &= \frac{(R_0 + R_1 \chi_{\perp}) I B}{t} = \frac{R_{H-eff} I}{t} B \end{aligned} \quad (6)$$

From the slope of the linear fit presented in Fig. 9b, the thickness $t = 480 \text{ nm}$ estimated from AFM images and the current $I = 50 \text{ nA}$ applied to the films, we can estimate

the effective Hall coefficient of the films in the interval of linear response as $R_{H-eff} \approx -0.29 \text{ m}^3/\text{C}$. The uncertainty in this measurement is determined mainly by the uncertainty in the thickness of the films. By considering an uncertainty in the thickness of the order of the rugosity measured by AFM, the uncertainty in R_{H-eff} is approximately of 3 %.

From our measurements is not possible to determine the ordinary Hall coefficient R_o by applying the relationship: $R_o = d\rho_H/d(\mu_0 H)|_{M_{\text{sat}}}$ because the magnetization M_{\perp} does not evidence total saturation in the range of magnetic flux density applied. In any case, the value of R_{H-eff} found in our films is almost six orders of magnitude higher than the values of $R_o = -0.0117 \times 10^{-6} \text{ m}^3/\text{C}$ and $R_A = -0.25 \times 10^{-6} \text{ m}^3/\text{C}$ reported by Murase and coworkers [18] in thin films obtained from $\text{Fe}_3\text{O}_4\text{-Fe}_2\text{TiO}_4$ solid solutions grown epitaxially, which is an indication of the small concentration of free electrons available in our films. This concentration is consistent with the important concentration of maghemite found in the Mössbauer measurements as well as the presence of polyacrylate in the precursor ferrofluid, both compounds having dielectric characteristics. The high effective Hall coefficient and the unsaturated response observed in the V_H vs B curve of the films are characteristics very suitable for their application as magnetic field sensors, because the signal to noise ratio of the voltage increases when the sensor has high sensitivity on a wide measurement range, where no saturation is present.

In the regions where the relation between V_H and B is less linear, other effects related to the granular and magnetic nature of the films become important, among them the grain boundaries, particle size distribution, canting of the magnetic moments in the surface of the films and magnetic anisotropies. However if the films are reproducible, a nonlinear relation between V_H and B is not an obstacle for their application as magnetic flux density sensors as long as the mathematical relation between these two variable can be well determined from previous characterization V_H and B measurements.

4 Conclusions

We have grown thin films by using the dip coating method and taking a ferrofluid of nanoparticles of magnetite-maghemite as precursor solution. The parameters of the dip coating process were configured in order to obtain thin films which covered almost uniformly the substrates. The films had an approximate thickness of 480 nm, a rugosity of 15 nm, an ohmic behavior for currents between 0 and 100 nA and a linear Hall response for magnetic flux densities between 0.15 and 0.30 T, with an effective Hall coefficient $R_H \approx 0.295 \text{ m}^3/\text{C}$ in that interval. The thin films obtained are promising for applications as sensing devices, such as Hall sensors and magneto-resistive devices, to the extent that their reproducibility and stability can be guaranteed, stage which is subject of future work.

References

1. Yang, S.-Y., Horng, H.-E., Hong, C.-Y., Yang, H.-C.: Structures, optical properties and potentially electro-optical applications of magnetic fluid films. *Tamkang J. Sci. Eng.* **5**(2), 85–93 (2002)
2. Silva, M.R., Martins, H., Nascimento, I., Baptista, J.M., Lobo Ribeiro, A., Santos, J.L., Jorge, P., Frazão, O.: Optical current sensors for high power systems: A review. *Appl. Sci.* **2**, 602–628 (2012)
3. Feng, J.S.-Y., Pashleyz, R.D., Nicolet, M.-A.: Magnetolectric properties of magnetite thin films. *J. Phys. C: Solid State Phys.* **8**, 1010–1022 (1975)
4. Wang, H.Q., Hoffman, J., Hong, X., Henrich, V.E., Ahn, C.H.: Planar hall effect in epitaxial thin films of magnetite. *J. Appl. Phys.* **101**, 09J507 (2007)

5. Fernández-Pacheco, A., Orna, J., De Teresa, J.M., Algarabel, P.A., Morellon, L., Pardo, J.A., Ibarra, M.R., Kampert, E., Zeitler, U.: High-field hall effect and magnetoresistance in Fe_3O_4 epitaxial thin films up to 30 Tesla. *Appl. Phys. Lett.* **95**, 262108 (2009)
6. Müller, G.M., Walowski, J., Djordjevic, M., Miao, G.-X., Gupta, A., Ramos, A.V., Gehrke, K., Moshnyaga, V., Samwer, K., Schmalhorst, J., Thomas, A., Hütten, A., Reiss, G., Moodera, S.J., Müinzenberg, M.: Spin polarization in half-metals probed by femtosecond spin excitation. *Nat. Mater.* **2341**, 56–61 (2008)
7. Zhang, C., Fan, C., Pan, L., Wang, F., Wu, P., Qiu, H., Gu, Y., Zhang, Y.: Magnetic and transport properties of magnetite thin films. *J. Magn. Magn. Mater.* **293**(2), 737–745 (2005)
8. Mi, W.B., Shen, J.J., Jiang, E.Y., Bai, H.L.: Microstructure, magnetic and magneto-transport properties of polycrystalline Fe_3O_4 films. *Acta Materialia* **55**, 1919–1926 (2007)
9. Furubayashi, T.: Magnetite films prepared by reactive evaporation. *J. Magn. Magn. Mater.* **vols. 1 of 2272–276, no SUPPL. 1**, 1–2 (2004)
10. Hu, X., Xu, M., Cui, X., Zhang, S.: Room-temperature magnetoresistance effects of Ag-added Fe_3O_4 films with single-domain grains. *Solid State Commun.* **142**(10), 595–599 (2007)
11. Tang, N., Zhong, W., Jiang, H., Wu, X., Liu, W., Du, Y.: Nanostructured magnetite (Fe_3O_4) thin films prepared by sol-gel method. *J. Magn. Magn. Mater.* **282**(0), 92–95 (2004)
12. Lin, C., Lee, C., Chiu, W.: Preparation and properties of poly (acrylic acid) oligomer stabilized superparamagnetic ferrofluid. *J. Colloid Interface Sci.* **291**, 411–420 (2005)
13. Velásquez, A.A., Urquijo, J.P., Gutiérrez, Y.: Diseño y construcción de un reactor mecatrónico para el crecimiento de películas delgadas por la técnica de recubrimiento por inmersión. *Ingeniería y Ciencia* **10**(20), 93–113 (2014)
14. Velásquez, A.A., Arroyave, M.: Implementation of a preamplifier-amplifier system for radiation detectors used in Mössbauer spectroscopy. *Hyp. Interact* **224**, 65–72 (2014)
15. Van der Pauw, L.J.: A method of measuring specific resistivity and Hall effect of discs of arbitrary shapes. *Philips Res. Reports: J. Theor. Exper. Res. Phys. Chem. Allied Fields* **13**(1), 1–9 (1958)
16. Vandenbergh, R., De Grave, E., De Bakker, P.M.A.: On the methodology of the analysis of Mössbauer spectra. *Hyp. Interact* **83**, 29–49 (1994)
17. Vandenbergh, R.E.: Mössbauer spectroscopy and applications in geology. In: International Training Centre for Post-Graduate Soil Scientists, p. 51. State University Gent, Belgium (1990)
18. Murase, H., Fujita, K., Murai, S., Tanaka, K.: Epitaxial growth of room-temperature ferrimagnetic semiconductor thin films based on Fe_3O_4 - Fe_2TiO_4 solid solution. *Mater. Trans.* **50**(5), 1076–1080 (2009)